Influence of Hydroxyapatite Particle Size on the Flowability of PLA/HA Filament

Nur Munirah Mustaza, Farrahshaida Mohd Salleh[*]*, Syahmin Ilyana Rahmat, Afeeqa Puteri Marzuki, Izdihar Tharazi, Muhammad Hussain Ismail, Bibi Intan Suraya Murat*
School of Mechanical Engineering, College of Engineering, Universiti Teknologi MARA, 40450 Shah Alam, Selangor, MALAYSIA
[*]*fshaida@uitm.edu.my*

ABSTRACT

Advanced bioactive ceramic materials, Hydroxyapatite (HA) and Polylactic Acid (PLA) are common in bone regeneration implants. As demand for customised implant products increases, research increasingly focuses on developing composite filament manufacturing technology. However, creating PLA/HA composite filament faces challenges, including clumping HA particles and uneven flowability. The brittleness of the filament properties makes it unsuitable for Fused Deposition Modelling (FDM) printing, causing inconsistent extrusion and reduced filament strength. The purpose of this study is to compare the effectiveness of microHAs (m-HAs) and nanoHAs (n-HAs) in the production of filament composite fibers, based on the flowability assessment. The particle size of the micro-HA was reduced to nano by a ball mill process using 4 mL ethanol and the ball-powder ratio of 5:1, which was verified by the particle size analyzer. The feedstock comprises 79.5 wt.% PLA, 19.5 wt.% HA and 1 wt.% impact modifier (IMK) was mixed and rheological tested (130 ℃ to 150 ℃, shear rate: 20-1000 s^{-1}) to achieve pseudoplastic behaviour (n<1). The rheological tests showed that both feedstocks exhibited pseudoplastic behaviour (n<1) across all temperatures studied. The properties of the feedstock were observed by scanning electron microscopy (SEM), and tensile tests evaluated the filament strength. The investigation found that nano-sized HA filament has 24% higher strength than micro-sized PLA/HA filament.

Keywords: *Polylactic Acid; Hydroxyapatite; Rheology; Filament Testing; 3D-Printing*

ISSN 1823-5514, eISSN 2550-164X

https://doi.org/10.24191/jmeche.v21i2.26261

Received for review: 2023-11-30
Accepted for publication: 2024-02-29
Published: 2024-04-15

Introduction

Digital fabrication technology, commonly known as 3D printing, has gained significant global utilization, particularly for mass customization and open-source design creation across many industries, including healthcare, automotive, aviation, and agriculture. This technology enables the layer-by-layer material deposition of objects directly from computer-aided design (CAD) models, showcasing its innovative and versatile nature [1]. This research focuses on using 3D printing in medical contexts, which led to numerous advancements in medical technology, including applications such as personalized implant materials, prosthetics, scaffolds, and orthotics [2]. The prevalent method for 3D printing that employs polymers to construct models or prototypes is recognized as Fused Deposition Modelling (FDM). This approach is straightforward and user-friendly guaranteeing efficient material usage and better physical results [3]. The fundamental principle underlying FDM involves raw materials' melting and subsequent shaping to create novel forms [4].

Polylactic acid (PLA) is a versatile biopolymer prominently utilized in the FDM process. For 3D printing evolution, PLA has emerged as a primary choice due to its user-friendly nature and lower printing temperature requirement. Its environmental sustainability stands out as it originates from renewable resources. Despite its reputation as a brittle substance with relatively low impact strength, PLA's mechanical attributes span from rigid, high-strength compositions to more pliable forms [5].

In bone repair, calcium phosphate has found extensive use due to its excellent biological properties [6]. Hydroxyapatite (HA) is the most stable among calcium phosphates, rendering it highly suitable for diverse medical applications, including dental restorations and implants. Its biocompatible ceramic properties have found extensive use in various medical fields, particularly in bone tissue. Leveraging its impressive mechanical strength as part of composite materials, HA has been harnessed for the regeneration of hard tissues [7]. However, its brittleness and limited mechanical strength have posed challenges, restricting its application in various scenarios. Incorporating an impact modifier (IMK) has been employed to enhance impact strength, ductility, and filament quality in compositions like PLA/micro-HA and PLA/nano-HA [8].

The combination of biopolymers and bioactive ceramics can achieve a balanced mechanical behaviour and bioactivity. The degradation of PLA, which results in acidic degradation, can lead to an acid-base imbalance on the defective side, and the addition of HA can neutralize this acidity [9]-[10]. The blending of PLA and HA can alleviate the negative aspects of the polymer, resulting in enhanced bioactivity, biocompatibility, high osteointegration, and osteoconductivity in the printed composite [9], [11]-[12]. As indicated by Bernardo et al. [11], the wettability of PLA can be improved by the presence

of HA, making the composite scaffold more hydrophilic. This property enhances cell proliferation and adhesion during the regeneration process, reducing the risks of infection and rejection to a minimum. The PLA/HA composite scaffold demonstrates congruence with natural bone tissue regarding structure, mechanical compatibility, and composition.

According to a study by Wu et al. [12], bending strength increases by 1.8-fold when the composite's micro-sized HA(*m*-HA) loading increases from 0 to 40 wt.%. However, at high concentrations of *m*-HA, the composite filament experiences a significant deterioration in printability. As a result, the commonly applied *m*-HA loading for FDM is 15 wt.%. Wang et al. [9] reported that the addition of nano-HA(*n*-HA) particles to the composite can enhance the mechanical behaviour of the PLA/*n*-HA composite, with *n*-HA loading generally kept lower than 15 wt.% compared to higher amounts of HA (20 wt.%, 30 wt.%, 40 wt.%, and 50 wt.%). This is because adding *n*-HA content negatively affects the ductility of PLA and renders the PLA/*n*-HA composite more prone to becoming brittle. Pandele et al. [13] indicated that adding 18 wt.% HA nanoparticles along with silver nanoparticles to the PLA matrix results in superior mechanical strength and excellent antibacterial properties, especially when compared to higher *n*-HA contents. Achieving a homogeneous dispersion and distribution of HA as an inorganic filler in the PLA matrix becomes difficult as the HA content increases. This is because higher HA content can lead to the formation of agglomerations within the composite, diminishing the shielding effect of the particles. Therefore, the optimal composition of HA for this study is determined to be 10 wt.%, which is believed to exert a maximum impact on the composite material.

Based on the comprehensive analysis of the literature, it is apparent that there is a gap in research addressing the influence of varying particle sizes of HA in a PLA matrix. Most studies instead utilized a uniform particle size of HA, whether in micro or nano forms [7], [9]-[10]. Particle size is pivotal as a reinforcing element in composites, significantly influencing their overall quality. Key parameters in particle size analysis include surface area, dimensions, projected area, volume, or cross-sectional area. Different particle sizes exhibit distinct functions. For instance, smaller particles have a larger exposed surface area interacting with the polymer matrix, enhancing dispersibility. This, in turn, contributes to greater mechanical strength compared to smaller particle sizes. Therefore, it is imperative to delve further into understanding the impact of different particle sizes of HA on composite materials. In this study, the utilization of IMK is anticipated to yield additional ductility to the composite material.

This study aims to observe the flow behaviour of the composite through the determination of the flow behaviour index, denoted as '*n*', across a range of temperatures of both micro and nano-composite material. The tensile test was conducted on both composite filaments. This test was performed to ascertain which type of composite, whether incorporating micro-sized or nano-sized HA

particles, exhibited superior strength. The study provides insights into the potential advantages of utilizing either *m*-HA or *n*-HA particles for reinforcing PLA-based composites.

Methodology

Ball milling

The process involved the utilization of a Fritsch Planetary Ball Mill Machine to synthesize *n*-HA through a wet milling method. This approach aimed to transform *m*-HA into *n*-HA particles, employing a grinding aid solution consisting of ethanol (C_2H_6O). This ethanol solution served the purpose of reducing the size of HA particles and preventing their agglomeration [14]. Both the ball mill jar, and the grinding media (balls) are alumina-type. During the process, the ball mill rotated at a speed of 150 revolutions per minute (rpm) and operated for 6 hours per session, maintaining a ball-to-powder ratio (BPR) of 5:1. The ball milling procedure was repeated five times to achieve the desired quantity of approximately 400 g of *n*-HA. The size of the milled HA particles was determined using a particle size analyzer to ascertain the resulting size of the *n*-HA particles obtained accurately.

Material characterization

Four different materials characterization analyses were conducted based on the respective materials: raw materials (PLA, HA, and IMK), as well as their composite. These analyses encompassed particle size distribution, thermal behaviour, morphology, and density. Two types of particle size analysers were employed: the Malvern Panalytical Mastersizer 2000 covering a size range of 0.02 to 2000 microns, and the Zetasizer Nano ZS with a range of 0.3 nm to 10 microns. Both analysers were used to assess the sizes of micro and nano-size HA particles. The standard refractive index (RI) value for HA is 1.651. Differential scanning calorimetry (DSC) is a thermal analysis method utilized to assess material characteristics like crystallization temperature, glass transition, and melting point. The technique employs pyrolysis nitrogen gas, with a heating rate of 10 ºC/min and a temperature range from 27 ºC to 500 ºC. Scanning Electron Microscopy (SEM) is commonly employed to produce detailed images of object shapes, aiding in material characterization by revealing particle attributes such as size, shape, surface structure, porosity, composition, and defects. The density of both composite feedstocks was determined using the Archimedes principal method [15].

Mixing and blending

The Internal Mixer Rheomix 600 machine was employed to mix and blend the materials for feedstock production. The composition for both composite materials (PLA/micro-HA and PLA/nano-HA) with added impact modifier

(IMK) was identical: 79.5 wt.% PLA, 19.5 wt.% HA, and 1 wt.% IMK. Initially, the temperature and speed were set at 190 ºC and 15 rpm, respectively. Half of the PLA was added to the tank and mixing began. After three minutes, the remaining PLA poured, and the speed was increased to 30 rpm. Within two more minutes, the speed was raised further to 45 rpm, and then IMK was added to the tank. Finally, HA powder was incorporated at 60 rpm. This blending process lasted around 45 minutes on average to ensure thorough homogenization of the feedstocks. Subsequently, a jaw crusher was used to break down the solidified feedstocks into granules. This mixing procedure was repeated five times for each composite, generating approximately 350 g of composite granules.

Rheological analysis

The Rosand Capillary Rheometer machine was utilized to assess the elasticity and shear viscosity of the materials. Rheological properties are affected by factors like shear rate, pressure, and temperature. In the rheological test, the shear rate varied from 20 s^{-1} to 1000 s^{-1}, press pressure of 0.1 MPA and a 1 mm diameter of die size. The testing was carried out at temperatures of 130 ºC, 140 ºC, and 150 ºC. The collected data encompassed shear viscosity, shear stress, and flow behaviour index (*n*).

Filament fabrication

Both composite filaments were produced using a twin-screw extruder (model: Haake Poly Lab OS; screw diameter: 16 mm, L/D: 25). Both composites were dried first at a temperature of 50 °C for 8 hours. The filaments were fabricated with a screw speed of 30 rpm, maintaining a feed zone temperature of 190 °C, compression zone temperature of 170 °C, metering zone temperature of 160 °C, and exiting the circular die with a diameter of 3 mm at a temperature of 150 °C. The resulting filament exhibited a fabricated diameter of 1.75 ± 0.1 mm.

Filament testing

The mechanical attributes of the filaments were assessed through a tensile test conducted on a Universal Testing Machine. The filament is approximately 110 mm in length and the gauge length is 60 mm. The test was carried out at a speed of 2 mm/min, utilizing a thickness equivalent to the composite filament's diameter of 1.75 mm. A load cell of 2.5 kN was employed.

Results and Discussion

Material characterization

The *m*-HA used in this study was sourced from the same batch as the HA employed in the study conducted by Marzuki et al. [15], wherein the particle

size of *m*-HA was reported as 8.32 μm. Based on this research, the graph of *m*-HA particle size distribution depicts a bimodal distribution. This dual-peak pattern in the frequency distribution suggests the presence of two distinct groups of particle sizes. Obtaining greater packing densities is possible when particle sizes are uneven [15]-[16]. The analysis of the particle size distribution for milled-HA, which was initially targeted to achieve a nano size, was conducted using the Zetasizer (nano) machine, and the results are presented in Table 1. The *Z*-average diameter value measured at 346 nm signifies the successful transformation of *m*-HA into the *n*-HA size range. In the realm of nanoparticles, the polydispersity index (PdI) serves as a gauge to assess the uniformity of particle solutions. It also provides insights into the consistency and efficacy of changes on particle surfaces and serves as an indicator of potential nanoparticle aggregation [17]. The PdI value spans a range from 0.0 (indicative of a fully uniform particle size sample) to 1. When the value trends toward 1, it suggests a broader size distribution within the sample. In the case of the measured *n*-HA sample, the PdI value was recorded at 0.487, falling within the preferred range. A PdI value below 0.5 is generally considered indicative of a favourable size distribution [18]. Figure 1 shows that the *n*-HA sample exhibits a bimodal distribution. This distinctive curve indicates the presence of both finer and coarser particles. The prominent peak on the right signifies the presence of larger particles, while the lower peak on the left corresponds to smaller particles. These two distinct peaks can be attributed to the uneven size distribution of the *m*-HA particles before the milling process.

Table 1: Particle size analysis of nano-HA

Particle name	Nano-hydroxyapatite (*n*-HA) powder
Particle RI	1.65
Temperature (ºC)	25.0
Count rate (kcps)	133.4
Cell description	Disposable sizing cuvette
Measurement position (mm)	4.65
Duration used (s)	80
Pdl	0.487
Z-average (d.nm)	346 nm

PLA/HA/IMK composite

DSC analysis was performed on both PLA and IMK samples. Figure 2 reveals the presence of two endothermic peaks corresponding to their respective glass transition temperature, T_g and melting points, T_m; while exothermic peak indicates crystallization temperature, T_c. In the case of PLA, the initial endothermic peak at 59.78 °C is attributed to the T_g process, signifying the transition of the polymer into a highly elastic state. The second endothermic peak observed at 154.82 °C indicates the T_m of the PLA pellet. A study by

Olam et al. [19] reported the DSC results for granular PLA, with T_g recorded at 60 °C and T_m at 155 °C. The trend and values of the T_g and T_m of PLA align closely with previous research findings. Minor discrepancies in these temperatures can be attributed to variations in the manufacturing process, which can slightly impact T_g and T_m [9]. PLA pellets do not exhibit a distinct crystallization curve (exothermic peak for T_c). This is attributed to PLA being a semicrystalline polymer known for its sluggish crystallization kinetics [20], along with its low crystalline content (approximately 3-5 wt.%) [21]. Moving on to IMK, the DSC analysis yields T_g and T_m of 60.65 ºC and 153.46 ºC, respectively. The T_m of the mixing process is set at higher or within the range of the melting temperature.

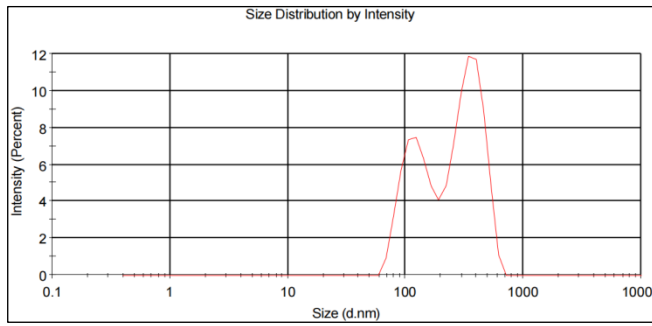

Figure 1: Plotted graph of intensity (%) against size (d.nm)

Moreover, the inclusion of HA and IMK in PLA influences the results of DSC analysis, affecting the values of T_g, T_c, and T_m , as depicted in Table 2. This influence arises from factors like the presence of crystalline substances and impurities in the input materials due to the composition (including HA and IMK), chain flexibility, intermolecular interactions, and molecular weight [22]. The T_g temperature of PLA/*m*-HA/IMK and PLA/*n*-HA/IMK were 51.08 ºC and 53.68 ºC, respectively, which is lower than the T_g of pure PLA pellets (59.78 ºC). The T_g value depends on the interface between the filler and polymer matrix, as well as the number of particles per unit volume in the composites [11]. The decrease in T_g of both composites indicates a softening of the polymer chain. This outcome results from the increased interfacial area caused by the presence of HA and IMK, leading to reduced mobility of polymer chains and consequently lowering T_g in comparison to pure PLA pellets. The variation in T_g values might be attributed to the structural relaxation peak, which can impact the accuracy of determining the inflection point [20]. The incorporation of HA into the polymer matrix results in the PLA composite having a crystallinity temperature, of T_c. This is attributed to the influence of HA particles acting as nucleating agents, leading to decreased

amorphous content and reduced free volume within the composite. Consequently, this trend impacts the mechanical properties, such as tensile strength, bending strength, and stiffness of the composite [11]. Both PLA/*m*-HA/IMK and PLA/*n*-HA/IMK exhibit higher T_m values compared to pure PLA pellets, measuring 157.76 ºC and 163 ºC, respectively. Both micro and nano-HA particles are aligned with the PLA chains, wherein the conversion of polymer solid state necessitates more energy and leads to an increase in the T*m* value.

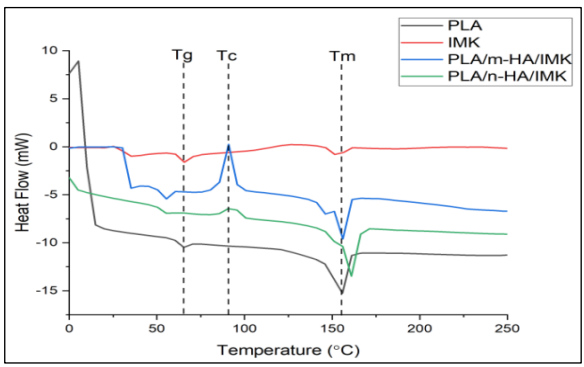

Figure 2: Graph of DSC analysis

Table 2: DSC analysis data

Sample	T_g (ºC)	T_m (ºC)	T_c (ºC)
Polylactic Acid (PLA) pellet	59.78	154.82	-
Impact modifier (IMK)	60.65	153.46	-
PLA/*m*-HA/IMK	51.08	157.76	91.52
PLA/*n*-HA/IMK	53.68	163.00	93.11

Figure 3a shows SEM images for PLA pellet, revealing a spherical form with a slightly textured surface. The *m*-HA powder, illustrated in Figure 3b, displays clumps of aggregated flakes, while the *n*-HA powder, shown in Figure 3c, exhibits an almost spherical or semicircular contour. The *n*-HA powder is accompanied by less stable clumps featuring small aggregates, enveloped by the smaller *m*-HA particles. In contrast, the *m*-HA's morphology presents a smoother and more regular appearance compared to the *n*-HA. This difference in morphology might be attributed to the manufacturing process used to create *n*-HA through ball milling, which could lead to uneven morphology results. Particles smaller than 1 μm in diameter usually aggregate into clusters, unless a surfactant is included to diminish the Van der Waals forces between them.

Despite thorough milling, agglomeration can persist and may become more prevalent [16].

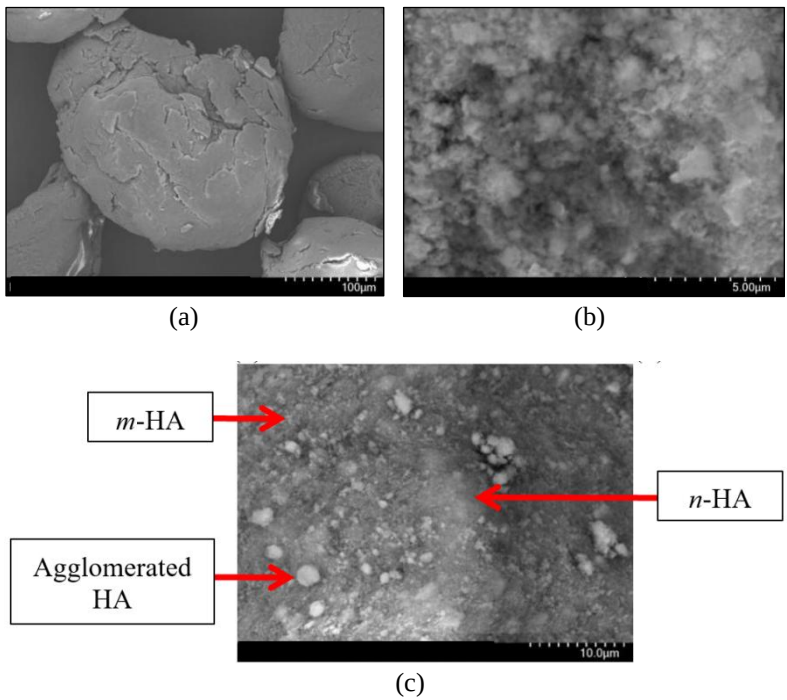

Figure 3: SEM images of raw materials; (a) PLA pellet (x300 magnification), (b) *m*-HA powder (x10000 magnification), and (c) *n*-HA powder (x3000 magnification)

The SEM images in Figure 4 reveal that both PLA/*m*-HA/IMK and PLA/*n*-HA/IMK composites illustrate that both types of HA particles were visible in a dispersed form. In the PLA/*n*-HA/IMK composite, the *n*-HA particles are distributed throughout the PLA matrix, showing irregular clustering regarding *n*-HA particle size, with some instances of agglomeration present. Conversely, the *m*-HA particles in the PLA matrix display more oversized agglomerates, leading to the PLA/*m*-HA/IMK composite having a rougher surface and slightly structured fracturing pattern.

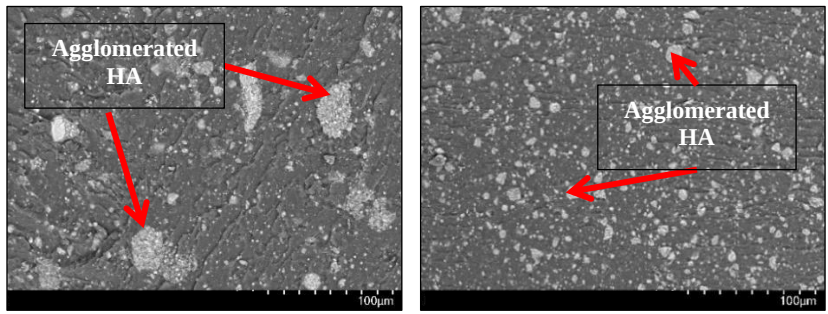

(a) (b)

Figure 4: SEM images of composites (a) PLA/*m*-HA/IMK (x500 magnification), and (b) PLA/*n*-HA/IMK (x500 magnification)

The density of PLA measured during the experiment was 1.2819 g/cm^3. Theoretically, PLA's density is 1.3 g/cm^3 [23]. The *m*-HA powder had a density of 3.356 g/cm^3, while the nano-HA density was 2.9689 g/cm^3. The theoretical density of HA powder is 3.16 g/cm^3, where it is unaffected by particle size [24]. The variation in both micro and nano-HA density could be due to the physical characteristics of the HA powder, particularly its tendency to clump together. This clumping, known as agglomeration, is a natural result of cohesive forces or Van der Waals forces acting between fine particles. Fine particles are more prone to clumping due to the stronger influence of surface forces like physical-chemical attraction and repulsion, as opposed to gravitational forces, which have less impact on smaller particles. The difference between the experimental and theoretical density values, as shown in Table 3, is less than 10 %.

Table 3: Density data for all samples

Material	Experimental (g/cm^3)	Theoretical (g/cm^3)	Error (%)
PLA	1.2819	1.300	1.39
Micro-HA	3.3560	3.160	6.20
Nano-HA	2.9689	3.160	6.05
IMK	0.6527	0.700	6.76
PLA/*m*-HA/IMK	1.3617	1.657	17.82
PLA/*n*-HA/IMK	1.3999	1.657	15.52

The measured density of PLA/*m*-HA/IMK composite was 1.3617 g/cm^3; while for PLA/*n*-HA/IMK composite was 1.3999 g/cm^3. The inclusion of both sizes of HA and IMK particles in the PLA matrix led to a higher density than pure PLA. These results align with the findings of Solechan et al. [25], where a 20% HA addition to a PLA/PCL matrix resulted in a density of 1.36

g/cm³. The addition of *n*-HA resulted in a higher density compared to the addition of *m*-HA. This is likely due to the strong bonding of *n*-HA particles within the PLA matrix, involving chemical changes during fabrication. The *n*-HA becomes absorbed into the PLA matrix, filling voids and increasing the density. This increase in density contributes to a reduction in voids within the composite, thereby enhancing its mechanical strength [3], [26]-[27]. Furthermore, the theoretical density of both composites was determined using the rule of mixture, resulting in a calculated value of 1.657 g/cm³, which was higher than the experimental density. This occurs because the composite's theoretical density calculation assumes the filler's complete filling of the matrix space. Nevertheless, achieving a composite without pores and voids poses a practical challenge. The formation of pores in the composite weakens the bond between the filler and the matrix, leading to a decrease in composite density. Additionally, the agglomeration of HA particles in the PLA matrix contributes to a reduction in composite density, as evident in SEM images. The percentage error in density for both composites remain below 18% as shown in Table 3.

Rheological analysis

The rheological behaviour of both PLA/*m*-HA/IMK and PLA/*n*-HA/IMK composites was analysed by plotting the shear viscosity against the shear rate at three different temperatures: 130 °C, 140 °C, and 150 °C, as shown in Figure 5. The graph for both composites exhibited a decrease in shear viscosity as the shear rate increased. This characteristic indicates shear thinning, also known as pseudoplastic behaviour. This phenomenon occurs due to the alignment of polymer chains induced at higher shear rates, which reduces the material's resistance to flow [28]. Pseudoplastic behaviour is desirable in 3D printing as it facilitates the extrusion of the material. The material's flowability becomes easier when viscosity is low enough at high shear rates within the nozzle. Consequently, the extruded pressure decreases. Additionally, this behaviour ensures that the printed samples maintain good shape stability without defects during the deposition process. This behaviour is marked by a drop-in shear rate exponentially, accompanied by a sudden increase in viscosity at the nozzle exit [29].

The viscosity of the PLA/*n*-HA/IMK composite is observed to be higher than PLA/*m*-HA/IMK composite across all three temperatures, as depicted in the graph below. This higher viscosity is attributed to the smaller particle size of *n*-HA, which provides a larger surface area and intensifies interparticle friction within the polymer matrix [30]. Additionally, the bimodal distribution of particle sizes in Figure 1 reveals variations in both fine and larger particle sizes of *n*-HA. This bimodal distribution results in a higher composite density in the PLA/*n*-HA/IMK composite, leading to superior viscosity compared to the PLA/*m*-HA/IMK composite [31]. Conversely, the PLA/*m*-HA/IMK composite exhibits larger agglomerations of *m*-HA, as evident in Figure 4,

along with a lower composite density. This configuration reduces interparticle friction, resulting in lower viscosity. Overall, the observed differences in particle sizes and agglomeration patterns contribute to the divergent viscosities between the two composites.

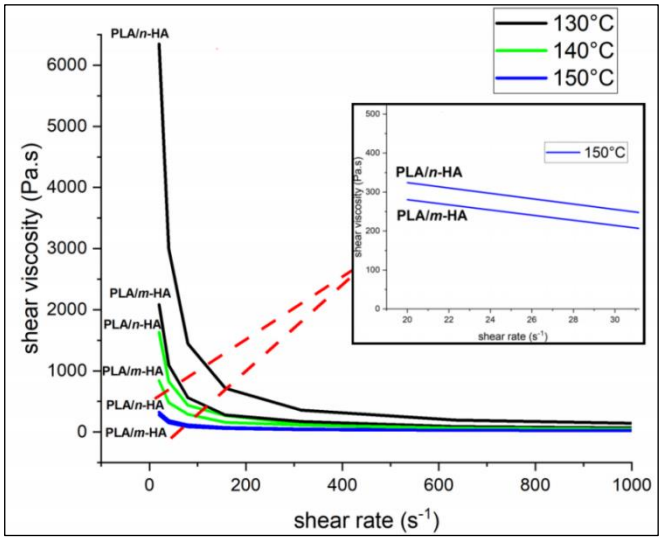

Figure 5: Graph of shear viscosity *vs.* shear rate of PLA/*m*-HA/IMK and PLA/*n*-HA/IMK at various temperatures

The flow behaviour index, *n* is applied to differentiate and quantify the extent of the pseudoplastic behaviour exhibited in Figures 6 and 7. This occurs when the value of *n* is less than 1, as described by the Power-Law equation (Equation (1)); where η represents viscosity, K stands for consistency, γ represents shear rate, and *n* signifies the exponent, which is the flow behaviour index.

$$\eta = K\gamma^{n-1} \quad (1)$$

Observing the values of *n* for both PLA/*m*-HA/IMK and PLA/*n*-HA/IMK at all three temperatures in Table 4, it becomes evident that both composites exhibit pseudoplastic behaviour, as indicated by *n* values less than 1. Particularly, at temperatures of 130 °C and 140 °C, the *n* values were significantly lower for both composites. These low *n* values result in high shear sensitivity, causing the shear rate and viscosity to change rapidly [32]. Notably, PLA/*m*-HA/IMK and PLA/*n*-HA/IMK composites show the highest *n* values at 150 °C, which are 0.33 and 0.333, respectively. At high

temperatures, the presence of hydroxyl (OH-) groups in HA accelerates the deterioration of the composites, resulting in a noticeable reduction in their viscosity [33]. The difference in the *n* values of both composites at 150 °C is not significant, indicating that the *n* value is not greatly affected by the different particle sizes in the composite. However, at a shear rate of 20 s^{-1} and a temperature of 150 °C, the PLA/*n*-HA/IMK composite exhibits a higher viscosity, measuring 324.11 Pa.s compared to the PLA/*m*-HA/IMK composite, 280.44 Pa.s. This is attributed to the smaller particle size of *n*-HA, which results in a larger surface area per unit volume. This characteristic increases interactions with the polymer matrix and generates more friction within the composite, resulting in higher viscosity [34]. Overall, the viscosity results for both composites at all temperatures met the suggested viscosity range for FDM 3D printing, which is between 10^2 and 10^5 Pa.s [35]. Therefore, the temperature of 150 °C will be used for filament production with a 1.75 mm die based on rheological analysis, as it exhibits a more pronounced shear thinning behaviour at this temperature.

Table 4: Flow behaviour index, *n* of feedstocks at different temperatures

Feedstocks	Temperature (ºC)	Flow behaviour index, *n*	Viscosity @ shear rate 20 s^{-1}
PLA/*m*-HA/IMK	130	0.259	2085.17
	140	0.147	841.86
	150	0.33	280.44
PLA/*n*-HA/IMK	130	0.052	6346.54
	140	0.159	1631.1
	150	0.333	324.11

PLA/HA/IMK filament

The morphology of both composite filaments was examined using SEM, as depicted in Figure 6. It is evident that both filaments contain numerous small and bright particles uniformly dispersed within the PLA matrix, representing HA. Additionally, both filaments display rough surfaces as a result of incorporating a higher content of HA particles. Furthermore, there are pores of various sizes (micro and macro-pores) present in both filaments, with prominent macro-pores observed in the PLA/*m*-HA/IMK filament. The formation of these pores may be linked to the reorientation of HA particles during the filament extrusion process. When HA particles encounter shear forces from the PLA matrix, they do not align perfectly with the flow direction, which results in the formation of pores [36]. The PLA/*m*-HA/IMK filament exhibits obvious longitudinal cracking, which can be attributed to the shear stresses applied at the nozzle tip experienced by the *m*-HA particles during the filament extrusion process and the interaction between micron-sized HA particles intensifies, also leading to the formation of crack on the filament

surface [36]-[37]. Additionally, it is evident that the PLA/*m*-HA/IMK filament shows agglomeration of *m*-HA particles, a result of the initial formation of *m*-HA itself. This results in an uneven circular shape of the PLA/*m*-HA/IMK filament with extensive clusters of *m*-HA particles on the outer surface, owing to the lower flowability of irregularly shaped particles.

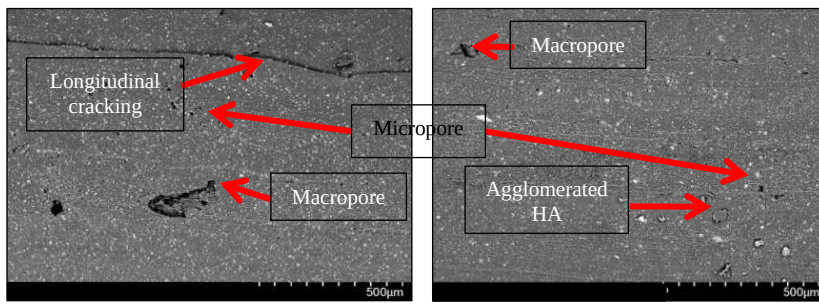

(a) (b)

Figure 6: SEM images of filaments; (a) PLA/*m*-HA/IMK (x100 magnification), and (b) PLA/*n*-HA/IMK (x100 magnification)

The tensile tests were conducted on both composite filaments, and the results are illustrated in Figure 7, with corresponding data presented in Table 5. It is evident that both composite filaments display similar stress-strain curve behaviours, characterized by steep and linear initial sections followed by a sudden end. The curves commence with a linear elastic phase upon the application of stress, indicating proportional deformation to the applied load and a return to their original shape upon load removal. The slope of the linear elastic region represents a modulus of resilience, commonly known as Young's modulus (*E*). The *E* for the PLA/*m*-HA/IMK composite filament is recorded as 8.16 MPa, notably lower than the 37.9 MPa observed for the PLA/*n*-HA/IMK composite filament. As the applied load surpasses a certain threshold, both filament materials reach an abrupt endpoint without significant plastic deformation. This signifies an early fracture point in the stress-strain curve, known as the Ultimate Tensile Stress (*UTS*). The PLA/*n*-HA/IMK composite filament exhibits a higher *UTS* at 0.563 MPa compared to the PLA/*m*-HA/IMK filament at 0.455 MPa. This observation indicates that both composite filaments exhibit brittle material characteristics, demonstrating low strain fracture behaviour, minimal energy absorption, and limited plastic deformation, as evident in both curves. This behaviour is attributed to the constrained dislocations within the crystal structure of the composite materials.

The increase in both *UTS* and *E* for the PLA/*n*-HA/IMK composite filament can be attributed to the reinforcing effect of *n*-HA and its smaller particle size, which results in a larger surface area and better integration within

the interstitial spaces of the PLA matrix, unlike the impact of *m*-HA. The lower *UTS* and *E* values for PLA/*m*-HA/IMK can be explained by the presence of *m*-HA, which acts as a local strain concentrator within the PLA matrix, along with the cluster aggregation of *m*-HA [13]. Besides, the prominent macropores and noticeable longitudinal cracking in the filament, as observed and mentioned in the SEM images above, make it prone to fracture and consequently result in reduced mechanical strength. Therefore, it is evident that the mechanical properties of composite filament materials depend on the characteristics of the filler, the homogeneity of dispersion morphology and interfacial properties between the filler and polymer matrix.

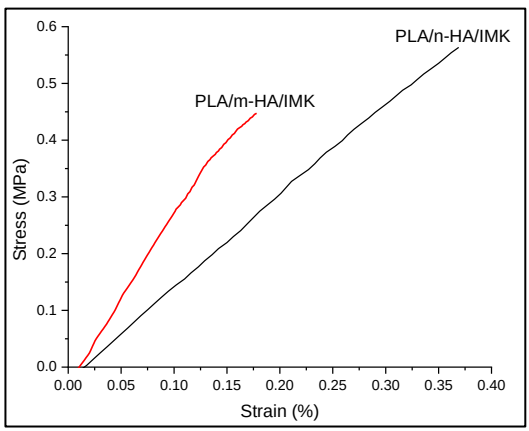

Figure 7: Graph of stress against strain of both composite filaments

The IMK appears to be more effective in enhancing the filament's elasticity when combined with *n*-HA. This may be attributed to *n*-HA smaller particle size, larger surface area, and the nearly spherical shape of morphological particles, which facilitate better interaction with the PLA matrix. Furthermore, to further enhance the elasticity value of composite filaments, the IMK content can be increased beyond 1 wt.% for future studies.

Nevertheless, the mechanical strength exhibited by both composite filaments is not comparable and significantly lower than the mechanical properties of the commercially available PLA filaments. According to Letcher et al. [38], the ultimate strain of PLA filament at a displacement rate of 5 mm/min was 16.0%, which is higher than the PLA/*m*-HA/IMK and PLA/*n*-HA/IMK composite filaments, recorded at 0.178% and 0.369%, respectively. This difference can be attributed to the properties of the raw PLA pellets used in this study. The purchased PLA pellets have a low molecular weight of 30 kg/mol. PLA with a molecular weight below 40 kg/mol exhibits brittle behavior, low melt viscosity, and a good ability for movement [39]-[40].

Furthermore, commercial PLA filaments are often blended with undisclosed additives including copolymer addition, carbon fiber, wood fiber and more. In addition, PLA is sourced from various fermented plant starches such as corn starch, sugarcane, cassava, and more. Different sources of PLA can result in varied PLA properties. Therefore, the disparity between commercial PLA and composite filaments can be attributed to the diverse factors influencing their properties.

Table 5: Data of tensile test of both composite filaments

Properties	PLA/*m*-HA/IMK	PLA/*n*-HA/IMK
Ultimate tensile stress (MPa)	0.455 ± 0.41	0.563 ± 0.09
Ultimate strain (%)	0.178 ± 0.07	0.369 ± 0.26
Young's modulus (MPa)	8.16 ± 10.25	37.9 ± 13.31

Conclusion

In conclusion, wet milling with ethanol as a grinding aid solution successfully reduced *m*-HA to *n*-HA, with a final nano-sized particle of 356.9 nm utilizing the ball milling approach. Both composite filaments were fabricated using the optimal temperature of 150 °C, as determined from rheological analysis, where both composites exhibited pseudoplastic behaviour with viscosity ranging between 10^2 to 10^5 Pa.s. Tensile tests revealed that the strength of the PLA/*n*-HA/IMK filament was 24% higher than that of the PLA/*m*-HA/IMK filament. Therefore, *n*-HA particles demonstrate superior behaviour and have the potential to serve as excellent constituents in polymer-ceramic composites, offering a viable alternative for bone replacement through the Fused Deposition Modeling (FDM) approach.

Contributions of Authors

All authors have performed their respective roles fairly, contributing to excellent collaboration. Furthermore, all authors have diligently reviewed and approved the final work of this paper.

Funding

Appreciation is extended for the financial support provided by the Ministry of Higher Education through the Fundamental Research Grant Scheme (FRGS/1/2021/WAB09/UITM/02/2) and SRP Grant (UI-UiTM BISA) under Grant No. 100-RMC 5/3/SRP (049/2021).

Conflict of Interests

One of the authors, Izdihar Tharazi, is a section editor of the Journal of Mechanical Engineering (JMechE). The author has no other conflict of interest to note.

Acknowledgement

The acknowledgement is extended to Gaia Plas Bhd. for their willingness to collaborate on this study, and College of Engineering, UiTM Shah Alam, for facilitating the use of laboratory facilities.

References

[1] N. Shahrubudin, T. C. Lee, and R. Ramlan, "An overview on 3D printing technology: technological, materials and applications," *Procedia Manufacturing*, vol. 35, pp. 1286-1296, 2019. https://doi.org/10.1016/j.promfg.2019.06.089

[2] Q. Yan, H. Dong, J. Su, J. Han, B. Song, Q. Wei, and Y. Shi, "A review of 3D printing technology for medical applications", *Engineering*, vol. 4, no. 5, pp. 729-734, 2018. https://doi.org/10.1016/j.eng.2018.07.021

[3] J. Mogan, W. S. W. Harun, K. Kadirgama, D. Ramasamy, F. M. Foudzi, A. B. Sulong, F. Tarlochan, and F. Ahmad "Fused deposition modelling of polymer composite: A Progress", *Polymers*, vol. 15, no. 1, p. 28, 2023. https://doi.org/10.3390/polym15010028

[4] T. N. A. T. Rahim, A. M. Abdullah, and H. M. Akil, "Recent developements in fused deposition modelling-based 3D printing of polymers and their composites", *Polymer Reviews*, vol. 59, no. 4. pp. 1-36, 2019. https://doi.org/10.1080/15583724.2019.1597883

[5] R. Miclaus, A. Repanovici, and N. Roman, "Biomaterials: Polylactic acid and 3D printing processes for orthosis and prosthetic", *Materiale Plastice*, vol. 54, no. 1, pp. 98-102, 2018. https://doi.org/10.37358/MP.17.1.4794

[6] N. Mathiazhagan, S. Palaniyappan, and N. K. Sivakumar NK, "Effect of fused filament fabrication parameters on crashworthiness studies of hydroxyapatite particle reinforced PLA composite thin-walled tubes," *Journal of the Mechanical Behaviour of Biomedical Materials*, vol. 138, pp. 1-18, 2023. https://doi.org/10.1016/j.jmbbm.2022.105611

[7] S. Mondal, T. P. Nguyen, V. H. Pham, and G. Hoang, "Hydroxyapatite nano bioceramics optimized 3D printing poly lactic acid scaffold for bone tissue engineering applications", *Ceramics International*, vol. 46, no. 3, pp. 3443-3455, 2020.

https://doi.org/10.1016/j.ceramint.2019.10.057
[8] X. Xiao, V. S. Chevali, and H. Wang, "Toughening of polylactide/bamboo powder biocomposite for 3D printing," *International Conference on Composite,* vol. 2, pp. 4927-4934, 2019. https://search.informit.org/doi/10.3316/informit.874003854188054
[9] W. Wang, B. Zhang, M. Li, C. Zhang, Y. Han, L. Wang, K. Wang, C. Zhou, L. Liu, Y. Fan, and X. Zhang, "3D printing of PLA/n-HA composite scaffolds with customized mechanical properties and biological functions for bone tissue engineering", *Composites Part B,* vol. 224, pp. 1-12, 2021. https://doi.org/10.1016/j.compositesb.2021.109192
[10] I. Gendvilience, E. Simoliunas, M. Alksne, S. Dibart, E. Jasiuniene, V. Cicenas, R. Jacobs, V. Bukelskiene, V. Rutkunas, "Effect of extracellular matrix and dental pulp stem cells on bone regeneration with 3D printed pla/ha composite scaffolds", *Cells & Materials,* vol. 41, pp. 204-215, 2021. https://doi.org/10.22203/eCM.V041A15
[11] M. P. Bernardo, B. C. R. D. Silva, and L. H. C. Mattoso, "Development of three-dimensional printing filaments based on poly(lactic acid)/hydroxyapatite composites with potential for tissue engineering," *Journal of Composite Materials,* vol. 1, pp. 12, 2021. https://doi.org/10.1177/0021998320988568
[12] D. Wu, A. Spanou, A. D. Escudero, and C. Persson, "3D-printed PLA/HA composite structures as synthetic trabecular bone: A feasibility study using fused deposition modeling," *Journal of the Mechanical Behaviour of Biomedical Materials,* vol. 103, pp. 1-10, 2020.https://doi.org/10.1016/j.jmbbm.2019.103608
[13] A. M. Pandele, A. Constantinescu, I. C. Radu, F. Miculescu, S. I Voicu, and L. T. Ciocan, "Synthesis and characterization of PLA-micro structured hydroxyapatite composite films", *Materials,* vol. 13, no. 274, pp. 1-13, 2020. https://doi.org/10.3390/ma13020274
[14] A. A. Eze, E. R. Sadiku, W. K. Kupolati, J. Synman, J. M. Ndambuki, T. Jamiru, M. O. Durowoju, I. D. Ibrahim, M. B. Shongwe, and D. A. Desai, "Wet ball milling of niobium by using ethanol, determination of the crystallite size and microstuctures", *Scientific Reports,* vol. 11, no. 22422, pp. 1-8, 2021. https://doi.org/10.1038/s41598-021-01916-w
[15] A. P. Marzuki, F. M. Salleh, M. N. S. Rosli, I. Tharazi, A. H. Abdullah, and N. H. A. Halim, "Rheological, mechanical and physical properties of Poly-Lactic Acid (PLA)/Hydroxyapatite (HA) composites prepared by an injection moulding process," *Journal of Mechanical Engineering*, vol. 19, no. 2, pp. 17-39, 2022.
[16] B. C. Mutsuddy, and R. G. Ford, "Ceramic Injection Molding," 1st ed. London: Chapman & Hall, 1995.
[17] K. N. Clayton, J. W. Salameh, S. T. Wereley, and S. T. K. Ursem, "Physical characterization of nanoparticle size and surface modification

using particle scattering diffusometry", *Biomicrofluids*, vol. 10, no. 5, pp. 1-14, 2016. https://doi.org/10.1063/1.4962992

[18] Y. Byun, J. B. Hwang, S. H. Bang, D. Darby, K. Cooksey, P. L. Dawson, H. J. Park, and S. Whiteside, "Formulation and characterization of a-tocopherol loaded poly e-caprolactone (PCL) nanoparticles", *Food Science and Technology*, vol. 4, no. 1, pp. 24-48, 2011. https://doi.org/10.1016/j.lwt.2010.06.032

[19] M. Olam, and N. Tosun, "3D-printed polylactide/hydroxyapatite/titania composite filaments", *Materials Chemistry and Physics*, vol. 276, pp. 1-11, 2022. https://doi.org/10.1016/j.matchemphys.2021.125267

[20] C. E. Corcione, F. Scalera, F. Gervaso, F. Montagna, A. Sannino, and A. Maffezzoli, "One-step solvent-free process for the fabrication of high loaded PLA/HA composite filament for 3D printing", *Thermal Analysis and Calorimetry*, vol. 134, pp. 575-582, 2018. https://doi.org/10.1007/s10973-018-7155-5

[21] S. Fehri, P. Cinelli, M. B. Coltelli, I. Anguillesi, and A. Lazzeri, "Thermal properties of plasticized poly (Lactic Acid) (PLA) containing nucleating agent," *International Journal of Chemical Engineering and Applications*, vol. 7, no. 2, pp. 1-4, 2016.

[22] F. S. Senatov, K. V. Niaza, M. Y. Zadorozhnyy, A. V. Maksimkin, S. D. Kaloshkin, and Y. Z. Estrin, "Mechanical properties and shape memory effect of 3D-printed PLA-based porous scaffolds," J*ournal of the Mechanical Behaviour of Biomedical Materials*, vol. 57, pp. 139-148, 2016. https://dx.doi.org/10.1016/j.jmbbm.2015.11.036

[23] R. Spina, "Performance analysis of coloured PLA products with a fused filament fabrication process", *Polymers*, vol. 11, no. 12, pp. 1-16,2019. https://doi.org/10.3390/polym11121984

[24] P. Oberbek, T. Bolek, A. Chlanda, S. Hirano, S. Kusnieruk, J. R. Tylman,G. Nechyporenko, V. Zinchenko, W. Swieszkowski, and T. Puzyn, "Characterization and influence of hydroxyapatite nanopowders on living cells," B*eilstein Journal of Nanotechnology*, vol. 9, pp. 3079-3094, 2018. https://doi.org/10.3762/bjnano.9.286

[25] S. Solechan, A. Suprihanto, S. A. Widyanto, J. Triyono, D. F. Fitriyana, J. P. Siregar, and T. Cionita, "Characterization of PLA/PCL/Nano-Hydroxyapatite (n-HA) Biocomposites Prepared via Cold Isostatic Pressing", *Polymers*, vol. 15, no. 3, pp. 559, 2023. https://doi.org/10.3390/polym15030559

[26] M. M. Kareem, and K. E. Tanner, "Optimising micro-hydroxyapatite reinforced poly(lactide acid) electrospun scaffolds for bone tissue engineering," *Journal of Materials Science: Materials in Medicine*, vol. 31, no. 38, 2020. https://doi.org/10.1007/s10856-020-06376-8

[27] M. R. Assalam, R. Ismail, A. P. Bayuseno, and D. F. Fitriyana, "Pengaruh suhu pembuatan filamen biokomposit (PCL/PLA/HA) menggunakan mesin screw extruder," *Jurnal Teknik Mesin*, vol. 11,no. 3, pp. 11-16,

2023.
[28] S. Jackson, and T. Dickens, "Rheological and structural characterization of 3D-printable polymer electrolyte inks", *Polymer Testing,* vol. 104, pp. 1-11, 2021. https://doi.org/10.1016/j.polymertesting.2021.107377
[29] G. D. Goh, Y. L. Yap, H. J. K. J. Tan, S. L. Sing, G. L. Goh, and W. Y. Yeong, "Process–structure–properties in polymer additive manufacturing via material extrusion: A review", *Critical Reviews in Solid State and Materials Sciences,* vol. 45, pp. 113-133, 2020. https://doi.org/10.1080/10408436.2018.1549977
[30] R. M. German, and A. Bose, "Injection Molding of Metals and Ceramics," 1st Ed. United States: Metal Powder Industry, 1997.
[31] S. Enferad, J. Petit, C. Gaiani, V. Falk, J. Burgain, S. K. D. Richter, M. Jenny, "Effect of particle size and formulation on powder rheology", *Particulate Science and Technology*, vol. 39, no. 3, pp. 1-10, 2020. https://doi.org/10.1080/02726351.2020.1738605
[32] R. N. Ahmad, N. Muhamad, A. B. Sulong, A. Wahi, and F. M. Salleh, "Rheological properties of titanium niobium based feedstocks for metal injection moulding," *Journal of Mechanical Engineering,* vol. 2, no. 1, pp. 139-149, 2017.
[33] E. H. Backes, L. D. N. Lires, C. A. G. Beatrice, L. C. Costa, F. R. Passador, and L. A. Pessan, "Fabrication of biocompatible composites of Poly(lactic acid)/Hydroxyapatite envisioning medical applications", *Polymer Engineering and Science*, vol. 60, no. 3, pp. 636-644, 2020. https://doi.org/10.1002/pen.25322
[34] R. Arrigo, A. Frache, "FDM printability of PLA based-materials: The key role of the rheological behavior", *Polymers*, vol. 14, no. 1754, pp. 1-15, 2022. https://doi.org/10.3390/polym14091754
[35] M. Bragaglia, F. R. Lamastra, P. Russo, L. Vitiello, M. Rinaldi, F. Fabbrocino, and F. Nanni, "A comparison of thermally conductive polyamide 6-boron nitride composites produced via additive layer manufacturing and compression molding", *Polymer Composites*, vol. 42, no. 6, pp. 2751-2765, 2021, doi. 10.1002/pc.26010.
[36] R. Bakhshi, M. M. Zerankeshi, M. M. Dehdezi, R. Alizadeh, S. Labbaf, and P. Abachi P, "Additive manufacturing of PLA-Mg composite scaffolds for hard tissue engineering applications," *Journal of the Mechanical Behavior of Biomedical Materials,* vol. 138, pp. 1-13, 2023. https://doi.org/10.1016/j.jmbbm.2023.105655
[37] M. Topuz, "Hydroxyapatite - Al2O3 reinforced poly- (lactic acid) hybrid coatings on magnesium: Characterization, mechanical and in-vitro bioactivity properties", *Surfaces and Interfaces*, vol. 37, pp. 1-13, 2023. https://doi.org/10.1016/j.surfin.2023.102724
[38] T. Letcher, M. Waytashek, "Material property testing of 3D-printed specimen in PLA on an entry-level 3D printer," *Proceedings of the ASME 2014 IMECE2014,* vol. 2, pp. 1-8, 2014.

https://doi.org/10.1115/IMECE2014-39379

[39] D. Rasselet, A. Ruellan, A. Guinault, G. Miquelard-Garnier, C. Sollogoub, B. Fayolle, "Oxidative degradation of polylactide (PLA) and its effects on physical and mechanical properties," *European Polymer Journal*, vol. 50, pp. 109-116, 2014. https://doi.org/10.1016/j.eurpolymj.2013.10.011

[40] X. Zhao, J. Yu, X. Liang, Z. Huang, J. Li, S. Peng, "Crystallization behaviors regulations and mechanical performances enhancement approaches of polylactic acid (PLA) biodegradable materials modified by organic nucleating agents," *International Journal of Biological Macromolecules*, vol. 233, pp. 1-17, 2023. https://doi.org/10.1016/j.ijbiomac.2023.123581